Glider-Based Observations of CO_2 in the Labrador Sea

Nicolai von Oppeln-Bronikowski[1], Brad deYoung[1], Dariia Atamanchuk[2], and Douglas Wallace[2]

[1]Department of Physics and Physical Oceanography, Memorial University, 283 Prince Phillip Drive, St. John's, NL, A1B3X7, Canada

[2]Department of Oceanography, Dalhousie University, 1355 Oxford Street, Halifax, NS, B3H4R2, Canada

Correspondence: Nicolai von Oppeln-Bronikowski (nbronikowski@mun.ca)

Abstract. Ocean gliders can provide high spatial and temporal resolution data and target specific ocean regions at a low cost compared to ship-based measurements. An important gap, however, given the need for carbon measurements, is the lack of capable sensors for glider-based CO_2 measurements. We need to develop robust methods to evaluate novel CO_2 sensors for gliders. Here we present results from testing the performance of a novel CO_2 optode sensor (Atamanchuk et al., 2014), deployed on a Slocum glider, in the Labrador Sea and on the Newfoundland Shelf. This paper (1) investigates the performance of the CO_2 optode on two glider deployments; (2) demonstrates the utility of using the autonomous SeaCycler profiler mooring (Send et al., 2013; Atamanchuk et al., 2020) to improve in-situ sensor data; and (3) presents data from moored and mobile platforms to resolve fine scales of temporal and spatial variability of O_2 and pCO_2 in the Labrador Sea. The Aanderaa CO_2 optode is an early prototype sensor that has not undergone rigorous testing on a glider but is compact and uses little power. Our analysis shows that the sensor suffers from instability and slow response times(τ_{95}>100 s), affected by different behaviour in weak (<0.1 °C) vs. strong (>10 °C) temperature gradients. We compare the glider data with the SeaCycler O_2 and CO_2 data and estimate the glider data uncertainty as $\pm$ 6.14 μM and $\pm$ 44.01 μatm respectively. From the Labrador Sea data, we point to short time (<7 days) and distance (<15 km) scales as important drivers of change in this region.

1 Introduction

The ocean plays a crucial role in absorbing the effects of changes to the Earth's atmospheric composition due to anthropogenic activities. Roughly one-third of all human-made CO_2 (C_{ant}) released into the atmosphere since the beginning of the industrial revolution has been taken up by the ocean, a total of 155 ± 31 GtC as of 2010 (Khatiwala et al., 2013). For the decade 2009–2018 alone, the global ocean carbon sink absorbed 2.5 ± 0.6 GtC·yr^{-1}, against fossil fuel emissions of 9.5 ± 0.5 GtC·yr^{-1} (Friedlingstein et al., 2019). Ocean carbon sinks are not equally distributed across the globe. Very intense carbon sinks and regions of anthropogenic carbon storage are located in subpolar ocean regions (Volk and Hoffert, 1985; Sabine et al., 2004), such as the Labrador Sea in the North Atlantic (DeGrandpre et al., 2006) and the Southern Ocean's Weddell Sea (van Heuven

et al., 2014). Deep mixing in these regions is adding anthropogenic carbon to the deep ocean water mass transports, linking these high-latitude carbon pumps to the global ocean (Broecker, 1991; Fontela et al., 2016). Increased carbon storage in the ocean has, over the past decades, caused pH levels to drop in many places (Doney et al., 2009), at a rate of change that is faster than found in the geological record (Zeebe et al., 2016). Resulting ocean acidification (OA) has already severely impacted marine habitats worldwide, including such important ecosystems as the Great Barrier Reef (Cohen and Holcomb, 2009; Guinotte and Fabry, 2009).

Predicting shifts in future carbon uptake scenarios requires a detailed understanding of the processes driving uptake and distribution of absorbed carbon across all oceanic scales. We need to advance the global ocean carbon measurement system because existing observations are limited in coverage and quality (Borges et al., 2010; Okazaki et al., 2017). There have been recent advances in autonomous sampling strategies to expand, improve and build-on existing global biogeochemical observing networks (Johnson et al., 2009). The existing Argo float program is expanding, including biogeochemical (BGC-Argo) sensors measuring oxygen, nitrate, chlorophyll, turbidity, irradiance and pH. BGC-Argo aims to observe seasonal to decadal-scale variability, although currently only about 8% of Argo floats are equipped with biogeochemical sensors (Johnson et al., 2017; Li et al., 2019). Improvements in resolution and frequency of surface CO_2 measurements have also come from developing stable ship-based in-situ measurement systems installed on container ships and tankers with regular routes across ocean basins. These results made possible the creation of a $1°$ global resolution (up to $1/4°$ coastal zones) Surface Ocean CO_2 Atlas (Bakker et al., 2016). However, these data do not provide at-depth information needed to understand the localized processes that drive and shape the strength of carbon sink regions such as the Labrador Sea. Advances in glider technology and sensors (Rudnick, 2016; Testor et al., 2019) can help address those gaps.

Advancing glider-based measurements of CO_2 requires addressing key issues such as stability, responsiveness, compactness and power consumption. (Clarke et al., 2017a, b; Fritzsche et al., 2018). Another important factor is to ascertain the uncertainty of sensor-based observations (Newton et al., 2015). So far, most carbon glider observations are limited to testing, and there remain concerns about data quality. The most mature and commonly used type of in-situ CO_2 probe is based on infrared (IR) detection, such as the CONTROS Hydro C[TM] or Pro Oceanus CO_2-Pro CV[TM] sensors. Unfortunately, commercial IR based detection systems are not yet small enough to easily fit existing gliders or float designs. Long equilibration times make profiling applications of sensors extremely challenging, requiring detailed knowledge of response times and data processing (Fiedler et al., 2013; Atamanchuk et al., 2020). These sensors are also very power hungry compared to other sensors like optodes or CTD's, making battery-powered deployments challenging even for moored applications. Another approach to determining in-situ CO_2 is through pH measurements using established Total Alkalinity (TA) and Salinity (S) relationships (Takeshita et al., 2014). Saba et al. (2018) applied a novel ISFET pH sensor (Johnson et al., 2016) developed by MBARI with help from Sea-Bird Scientific on a glider. These tests showed remarkable response time characteristics and stability over periods of several weeks or longer.

Another candidate for glider carbon observations is the Aanderaa CO_2 optode sensor (Atamanchuk et al., 2014). It is nearly identical in size and power consumption to the commonly used oxygen optode by the same company but lacks prior glider testing. The optode detects the luminescent-quenching response from a CO_2 sensitive membrane. In general, there are multiple

challenges to using photo-chemical sensors on profiling applications Bittig et al. (2014): (1) placement of the sensor on the glider dictates boundary layer thickness and response time; (2) response time is non-linearly temperature-dependent and steep temperature gradients induce additive error; and (3) the sensor is highly dependent on prior foil calibration and can suffer from drift. In particular, the foil design has multiple temperature-dependent rate-limiting processes inside the foil to sense the ambient change in pH, which relates to changes in pCO_2 (Sergey Borisov, sergey.borisov@tugraz.at, *personal communications*). On the upside, the CO_2 optode is an attractive candidate for gliders due to its small size, ease of integration, and low power consumption, all similar to the Aanderaa oxygen optode. Because of the need for increased spatial and temporal resolution of CO_2 observations and the advantages gliders offer compared to other methods, assessing the CO_2 optode on a glider is an important step in furthering community knowledge on the current state of mobile CO_2 system technology.

In 2016, as part of the Ventilations, Interactions and Transports Across the Labrador Sea (VITALS) project, we devised an observing strategy to carry out novel in-situ observations to (1) reach the deep convection region with a glider to carry out sampling with the novel foil-based pCO_2 sensor from Aanderaa with minimal ship resources for launch and recovery; and (2) use measurements provided by an autonomous moored profiler - the SeaCycler (Send et al., 2013), carrying the larger payload CO_2-Pro CV instrument for glider in-situ calibration points. This mission attempted to use a moored sensing platform as an in-situ reference point for experimental sensors deployed on a glider to advance data quality and coherence of novel biogeochemical measurements. As technology plays a catch-up game, such mission concepts will be important in the next steps towards targeted oceanic carbon measurements. We re-deployed the glider in September 2018 on the Newfoundland Shelf, in Trinity Bay, to further test the concepts from VITALS, flying the glider near a small fishing boat from which reference casts were taken using a similar CO_2-Pro CV instrument. We utilize these two real ocean deployments to improve sensor characterization and the quality of the collected data. In this paper, we present the data and our analysis and discussion around three central questions:

- How suitable is the CO_2 optode for glider-based applications?

- How can multiple autonomous platforms be used to improve sensor data?

- How can combined data from moored and mobile platforms resolve scales of temporal and spatial variability?

Addressing these questions should improve and shape our plans for carbon observing systems utilizing glider and other platforms, especially as new sensors, are being developed.

2 Data and Methods

2.1 Labrador Sea Deployment

In fall 2016, a moored vertical profiler, the SeaCycler (Send et al., 2013; Atamanchuk et al., 2020) and a G2 Slocum glider were deployed into the central Labrador Sea near the longtime German deep convection mooring K1 (Figure 1). The K1 mooring, located about 25 km west of former OWS BRAVO (Avsic et al., 2006), has been deployed biennially since 1994 to monitor

90 activity in the central deep convection patch in the Labrador Sea (Lavender et al., 2002; Koelling et al., 2017). The objective of VITALS was to characterize the spatial and temporal structure of oxygen and CO_2 in the deep convection zone. Other activity in conjunction with VITALS, included a hydrographic section AR7W maintained by the Bedford Institute of Oceanography (BIO) and Argo floats released with several profiles captured near the SeaCycler site and the glider deployment area. Many observing efforts came together, utilizing multiple complementary efforts across different scientific programs, relying on traditional and

95 novel observational approaches.
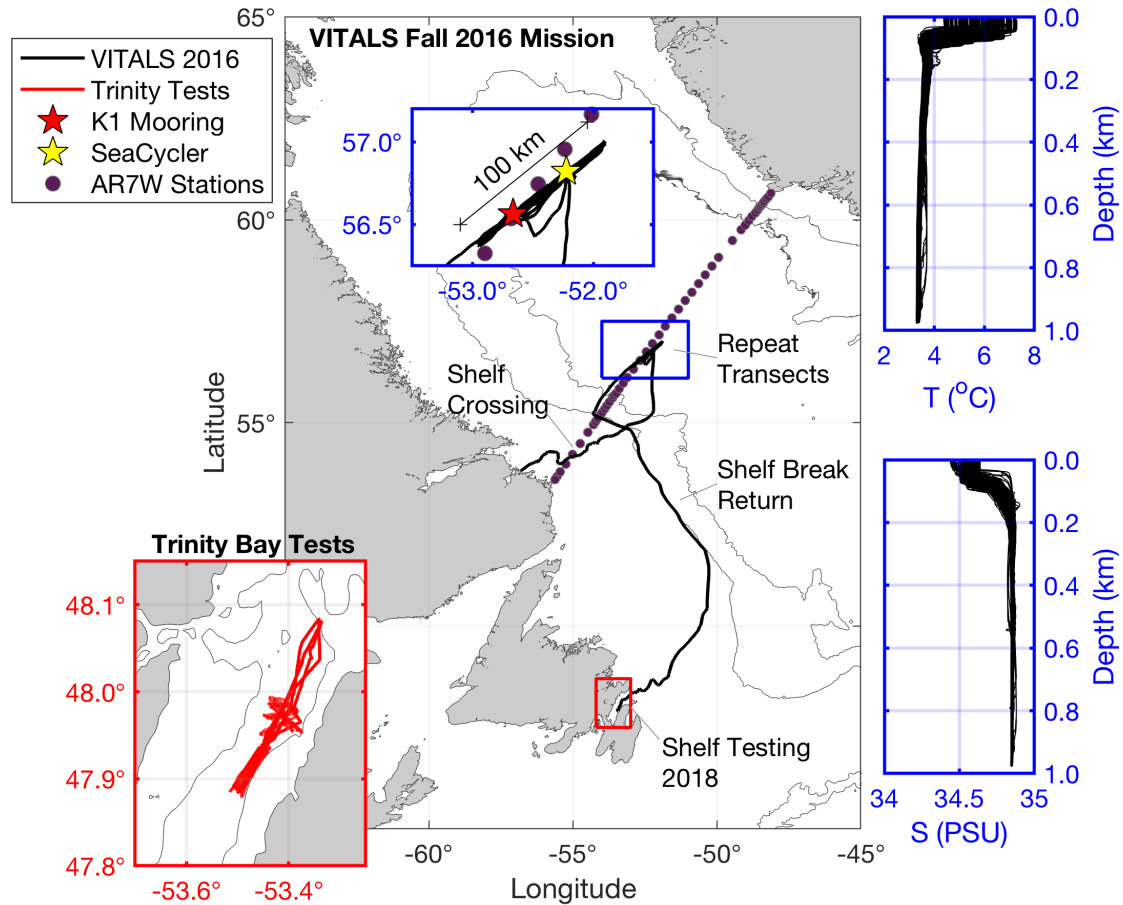
Figure 1. Map of data collection sites: main map (center) shows Ventilation, Interaction and Transport Across the Labrador Sea (VITALS) glider track with blue inset focusing on the repeat transects along the AR7W line. Contours are the 1500 m and 3000 m isobaths. Highlighted in blue are also the corresponding T–S profiles collected by the glider in that time period. The red inset map in the lower left shows the glider track from the 2018 glider CO_2 optode tests conducted in Trinity Bay, NL.

The SeaCycler was deployed near 52.22°W and 56.82°N, 30 km away from the German deep convection mooring K1 (52.66°W and 56.56°N) to improve the vertical and temporal characterization of O_2 and CO_2 cycling in this region. The

SeaCycler operation and deployment techniques are described in Send et al. (2013). It has an underwater winch assembly, parked at 160 m depth with an instrument float that can profile the top 150 m. A tethered communication allows for two-way telemetry over Iridium Satellite. Below the winch assembly, a single-point mooring line with instruments continues to the ocean depth of approximately 3500 m. For this deployment, the instrument float carried a CTD, velocity and various gas sensors, including oxygen sensors (Sea-Bird 43, Sea-Bird 63, Aanderaa 4330) and CO_2 optode prototype sensor 4797 as well as membrane equilibrator-based infrared (IR) CO_2 gas analyzer CO_2-Pro CV, based on non-dispersive infrared refraction (NDIR) technology made by Pro Oceanus Ltd, Canada (www.pro-oceanus.com). Previous tests with a similar sensor design showed excellent stability in multi-month vessel-underway missions (Jiang et al., 2014). The instrument float collected data over the top 150 m of ocean depth with an average resolution of 0.3 m from June 2016 to May 2017, while the Pro CV was sampling for 20 minutes at selected stop depths (10, 30, 60, 120 m) to allow equilibration with ambient seawater pCO_2. These stops resembled bottle stops done from ships with the water rosette to validate new sensors. The K1 mooring was also equipped with oxygen sensors to allow for later cross mooring comparisons. The SeaCycler data were corrected for sensor drift using pre- and post-deployment calibration of the sensors (Atamanchuk et al., 2020). The oxygen data were also corrected for a response time delay using the response time values from Bittig et al. (2014) and the algorithm described in Miloshevich et al. (2004). Overall the accuracy of the oxygen data was $2.89\pm4.17\ \mu M$ based on residuals between the upcast and discrete downcast data. The Pro CV had a zero-referencing routine that corrected the drift of the zero-point of the sensor Atamanchuk et al. (2020). Fully-equilibrated pCO_2 data were obtained by averaging the last 30s of the measurements at each stop depth. Accuracy of pCO_2 data was determined from the accuracy of the instrument, i.e. 0.5 % over the full range (0–1000 μatm) with an initial manufacturer quoted accuracy of $\pm2\ \mu$atm.

The glider (Unit 473) was deployed from the Labrador shelf to reach the K1 – SeaCycler site and complete 30 to 100 km long transects between the two moorings, collecting high-resolution spatial data. The glider was launched near Cartwright, Labrador, from a small fishing boat and reached the deep convection zone near K1 and SeaCycler early in October, sampling there until November 22. In total, the glider completed 18 full transects collecting valuable hydrographic and gas data. The modified glider with an extended battery bay carried Sea-Bird glider payload CTD and the Aanderaa Data Instruments (AADI) CO_2 optode prototype sensor (model 4797) described in Atamanchuk et al. (2014), and the well established Aanderaa oxygen Optode (Tengberg et al., 2006) model 4831, SN 333. Glider CTD manufacturer calibration showed an initial accuracy better than ±0.0005 S/M, ±0.005 °C and 0.1% of the total pressure range. The initial accuracy of the calibrated O_2 optode from the manufacturer was better than $\pm 4\ \mu M$. Accuracy of the CO_2 optode pre-deployment was unknown, but the accuracy range in Atamanchuk et al. (2014) is between ± 2–$75\ \mu$atm. The CO_2 optode (SN57) was equipped with a standard foil to enhance deployment stability. These optode sensors were mounted in the aft cone of the vehicle. Also, a thruster was installed to speed up the shelf's crossing and enable staircase profile sampling. The glider sampled in the central Labrador Sea for two months, limiting CO_2 optode profiles to the top 200 m to save energy. In December, the glider began its journey back to Newfoundland following the 1500 m isobath inside the Labrador Current and reaching Trinity Bay (see map) on December 31, 2016. The glider was flown along the shelf break to take advantage of the southward flowing Labrador Current. Before deployment on the

glider, the CO_2 optode underwent testing at the CERC.OCEAN laboratory at Dalhousie University to determine the calibration model fit for the optode sensor foil.

2.2 Trinity Bay Tests

135   After completing the VITALS mission, to further test all the characteristics of the new CO_2 optode under glider profiling tests, we conducted another study in Trinity Bay, Newfoundland. Trinity Bay is a deep inlet (up to 600 m) and can be reached easily from various coastal communities from a fishing boat. It is fed primarily by the cold Labrador Current waters and river runoff from the western side, making its surface waters fresh and deeper portions cold and highly oxygenated and nutrient-rich. The pooling of water in the deeper portion and surface freshwater support a stable density stratification (Schillinger et al., 2000;

140   Tittensor et al., 2002). Especially interesting for our optode tests are the large temperature gradients in the vertical of over 14 °C between the surface and 75 m depth. Trinity Bay has a cold water lens -1 °C between 70 m to 200 m depth (Figure 2d), and temperatures below 1 °C from 200 m to the bottom. In Trinity Bay, profiling through this lens leads to absolute temperature gradients of 10 °C or more in 200 s or less.
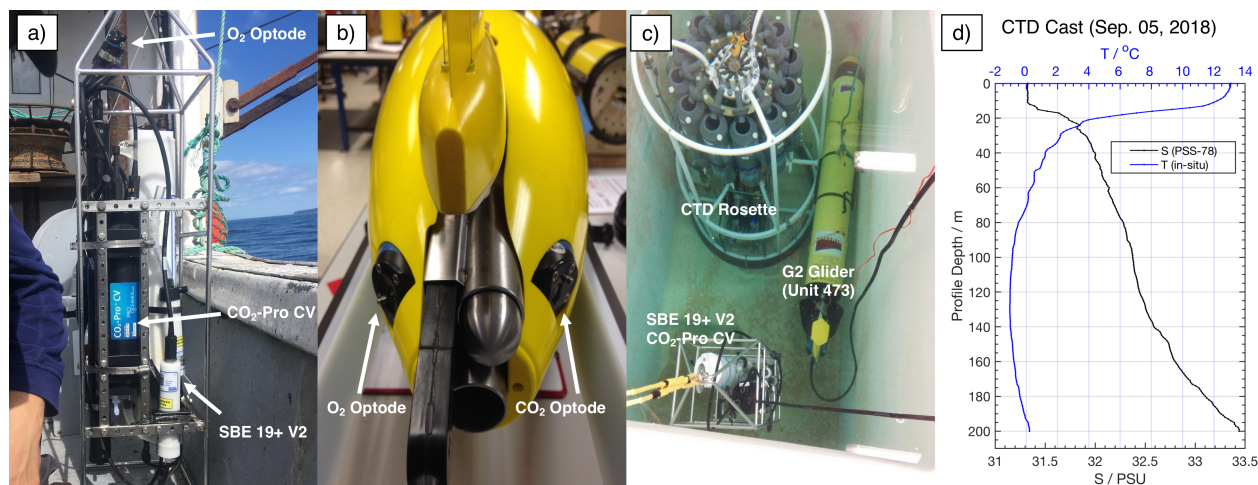
Figure 2. (a) Trinity Bay test reference CTD, (b) glider setup, (c) equipment tank testing in progress and (d) Average T–S structure observed from shipboard casts on September 5, 2018.

In Trinity Bay, we repeated the VITALS data comparison experiment on a smaller scale without using a SeaCycler. To

145   collect in-situ reference samples, we used a winch operated Sea-Bird 19+ V2 CTD mounted on a frame, together with a O_2 Optode (Model 4831, SN 333) and a CO_2-Pro CV. We repeated staircase missions as in VITALS and did extensive calibration of the sensor before and after the deployment. The glider was deployed from September 4–16, 2018. The setups for the external winch-operated CTD and glider are summarized in Figures 2a and 2b.

Pre-mission laboratory testing of the sensor and the glider allowed for instrument data quality control in this mission. The

150   glider CO_2 and O_2 optode sensors were calibrated at the CERC.OCEAN laboratory at Dalhousie University using a double-

Table 1. Sensor offsets from DFO Tank Tests August 27, 2018

(parameter)	($\bar{x} \pm 1$ STD)	(units)	(sensor make)
Slocum glider (Unit 473)			
T	0.0024 ± 0.0555	°C	SBE41cp
C	0.0019 ± 0.0033	S/m	"
O_2	14.05 ± 0.66	μM	Aanderaa 4831
CO_2	-461.14 ± 10.28	μatm	Aanderaa 4979
CTD–Pro CV system			
T	0.0255 ± 0.0555	°C	SBE19+ V2
C	0.0033 ± 0.0033	S/m	"
O_2	25.95 ± 0.66	μM	Aanderaa 4831
CO_2[*]	-51.45 ± 10.28	μatm	Pro CV

[*]Note: CO_2-Pro CV was located close to the tank's inlet which could be the cause of the large offset.

walled test tank, with simultaneous O_2 and CO_2 supply for rapid step changes in these variables. The optode sensor response in the range of -1.8 °C to 20 °C and O_2 concentrations ranging from 0 to 120% saturation and CO_2 concentrations from 100 to 3000 μatm were used to compute the CO_2 optode foil coefficients. Tests were initially done in freshwater and repeated for 35 ppt NaCl solution. Further, tests of glider sensors together with the CTD-Pro CV setup were done inside a saltwater tank at the Department of Fisheries and Oceans (DFO) in St. John's, Canada. The tank allows simultaneously submerging the glider, CTD-Pro CV setup and a CTD–rosette (SBE9) with Niskin bottles to obtain reference O_2, TA, DIC, T, S data. A summary of the water sample analysis and uncertainty is given in Appendix A. Based on the tank tests, we estimate initial sensor offsets for the glider and the CTD-Pro CV. Table 1 summarizes results from the DFO tank tests. Reported uncertainties are combined uncertainty of the measured offsets ($\bar{x}$) from tank tests, including the uncertainty from the lab-based results ($\pm$ 1 STD) and the manufacturer's sensor accuracy. STD in the text refers to the sample standard deviation. A picture of tank testing in progress is shown in Figure 2c. The location of the CO_2-Pro CV (bottom left) during the tank tests is close to an inlet, which may have caused a noticeable difference in CO_2 values. Before the deployment, we find an initial offset of -461.14 μatm for the glider CO_2 optode. However, the sensor had not yet undergone conditioning. Other sensors (CTD,O_2 optode) show good agreement between each other and with the collected water samples giving a good initial reference for the sensors.

2.3 Glider Data Processing

We processed glider science data, correcting the CTD-data for temperature-induced sensor lag, applying sequential comparison between glider profiles Garau et al. (2011). To correct the phase response lag in the glider oxygen data, we applied the model published in Bittig et al. (2014) using raw sensor phase angle output. Instead of using the built-in optode thermistor, we used the

lag-corrected CTD temperature readings interpolated to the optode measurements as in Gourcuff (2014). From the corrected phase readings, we computed the molar oxygen concentrations (μM or μmol/L) using (Uchida et al., 2008), with fit constants from a prior optode tank calibration. Trinity Bay, tank test and ship-based CTD profiles provided further calibration points at the start and end of the deployment.

For the CO_2 optode, there was some literature available for temperature-dependent response time corrections (Bittig et al., 2014). However, each sensor has its response time characteristic that must be determined before any field deployments. Due to the DLR technique in the foil and available field results, the sensor response is larger than the O_2 optode, which uses more straightforward foil chemistry. To correct for the long response time behaviour, we used a sequential time-lag correction (Equation 1) approach (Miloshevich et al., 2004), recently applied for an equilibrator type NDIR gas instrument (Fiedler et al., 2013). In Fiedler et al. (2013), the NDIR instrument was mounted on a profiling float, and response times are calculated to be on the order of 100–300s between surface and depth measurements.

$$c_{i+1}^{\text{cor}} = \frac{c_{i+1}^{\text{in situ}} - [c_i^{\text{in situ}} \exp(-\Delta t / \tau)]}{1 - exp(-\Delta t / \tau)} \tag{1}$$

Here $c^{\text{in situ}}$ is the raw and c^{cor} is the corrected sensor output at each time step i. The time constant τ can be computed by fitting an exponential model to the sensor response $x(t)$ (Equation 2) using fitting constants a, b at each time interval dt.

$$x(t) = (a - b) \exp(-dt / \tau) + b \tag{2}$$

Atamanchuk et al. (2014) provided a few values for the response time. Temperatures were much warmer than found in the Labrador Sea or Trinity Bay and did not provide response characterization for varying temperature gradients. Fiedler et al. (2013) used an exponential model (Equation 2) to compare his NDIR sensors response to zero-measurements (ZM). During ZM's, the sensor strips the gas stream of CO_2, and the resulting reading should be zero. The time response of the sensor and resulting reading after ZM were used to gauge the sensor's response to smaller gas gradients and drift of the gas detector itself. Because the optode sensor does not have the internal capability for independent referencing of the foil chemistry, we fitted the equation to the sensor response while the glider ascended or descended through the thermocline. Repeating this procedure for both glider deployments, we computed a temperature and response time-dependent set of values.

The staircase glider profiles in Trinity Bay were performed to help characterize sensor response to a broader set of positive and negative temperature gradients. Staircase profiles Figure 3, shows the least-squares fit for a single temperature gradient and optode response excursion. To compute the partial pressure of CO_2 (pCO$_2$) in micro-atmospheres (μatm) from the sensors corrected phase readings, we applied a calibration fit model from previous tank calibration done at CERC.OCEAN laboratory at Dalhousie University as was done in previous deployments of this sensor (Atamanchuk et al., 2015; Peeters et al., 2016). A testing regime of temperature and molar xCO$_2$ concentrations step changes, and sensors phase response readings were used to compute an 8-degree phase and 3-degree temperature model fit, which we applied to the sensor. The sensor data and calibration coefficients are available online (von Oppeln-Bronikowski, 2019).

The CO_2 optode sensor exhibits noticeable conditioning behaviour (Atamanchuk et al., 2015). After the sensor stabilized, we subtracted an offset (1275 μatm) for the VITALS deployment, based on the surface SeaCycler and atmospheric data, to
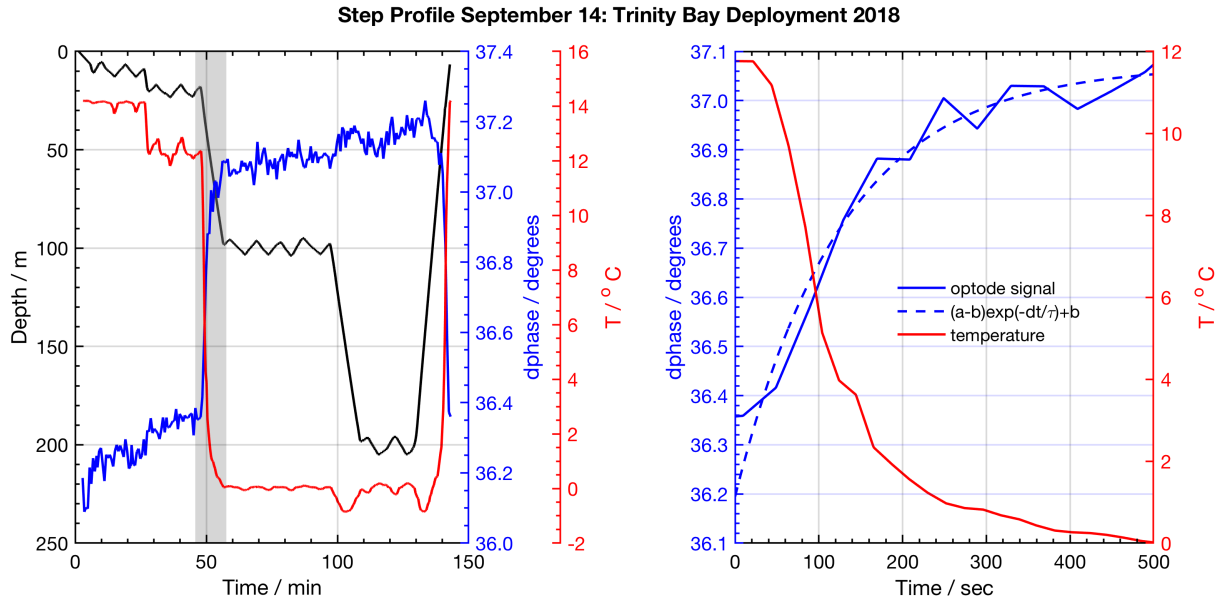
Figure 3. Example of a staircase profile used to quantify response time characteristics. Left panel shows glider staircase profile (black) overlaid with glider CTD temperature (red) and CO_2 optode signal (blue). Grey shaded area highlights an example episode of sensor response, shown in the right panel used to quantify the sensors response time and correct glider profiles. The exponential fit to the CO_2 optode response is shown (dashed blue line).

correct the optode sensor to ambient conditions. We estimated the time scale of conditioning by fitting an exponential curve to the optode data to find the time constant at which the sensor response plateaued. In the VITALS deployment, conditioning took almost a month into the deployment, while in Trinity Bay tests, the sensor response stabilized after four days (offset of

205   994 μatm). During the last 1.5 days of the Trinity Bay tests, the sensor displayed inconsistent behaviour with depth. Data from the final 1.5 days were excluded from further analysis. It is not clear what caused this change in the sensor's response. Perhaps cold temperatures in Trinity Bay (<-1°C) caused the foil to degrade.

To help with visualization, we bin averaged the data and mapped the data along isopycnals. For some cross-sectional plots, we also averaged data in depth-space or depth-time sections. To account for the gaps in observations, we preserved gaps larger

210   than 10 km and more prolonged than 4 days. Smaller gaps were linearly interpolated. A 3D boxcar filter was applied to smooth 5 km in the horizontal, 5 m depth, and 3-day in time, keeping with the observing gaps in the data because the glider occupied a section between K1 and SeaCycler every 2 to 3 days and gaps between profiles were 3 km on average.

To grid the sparse O_2 and pCO_2 glider observations for spatial-temporal data inter-comparison with SeaCycler, we deviated from linear interpolation. We used an objective interpolation method using a second-degree polynomial fitting distance weight-

215   ing scheme following Goodin et al. (1979). We gridded the sparse data on a 1-km by 1-day grid and then interpolated the data using an exponential weighting function $\exp\left(R_x^{-2} + R_y^{-2}\right)$ to fill in gaps. We determined influence radii of approximately 5 km

for O_2 and 20 km for pCO_2 measurements and cutoffs at 10 and 40 km respectively, based on the number of glider observations in the horizontal and along the time dimension. We set the cutoff radius at twice the spatial scale. Temporal scales are similar between the two data sets with an influence radius of 3 days and a cutoff of 6 days.

2.4 Shipboard CTD and Pro CV Casts

The Trinity Bay Tests CTD profiles together with O_2 optode and data from the Pro CV were processed by checking for outliers in the profiles. Despite the use of a pump, the Pro CV showed long signal equilibration periods (τ_{95} between 10 to 15 min). To compute the CO_2 levels for each time the CTD was parked at depth, we took the average of the CO_2-Pro CV values, once readings stabilized to within $\pm$ 6 ppm or twice the manufacturer's quoted instrument accuracy (0.5% of the total range 0 - 600 ppm). We developed a simple script that identified the first time window when the difference in sensor readings reached $\Delta CO_2 \leq 6$ ppm. Pro CV ZM's were subtracted from bottle stops to arrive at a high-quality in-situ referenced data set. We calculated the standard deviation for each set of averaged Pro CV measurements and flagged any data points as outliers when the standard deviation exceeded $\pm$ 6 ppm. Those data points were not included in the sensor data comparisons.

3 Results and Discussion

3.1 Glider-based CO_2 Optode Performance

Before this study, the CO_2 optode response had not studied on a glider, and little information was available about its response-time characteristics when profiling. We assess the sensor response time by fitting the raw "dphase" sensor signal (ϕ_{DLR}) with the earlier described exponential model (Equation 2) during periods when the glider traversed through temperature gradients. From Equation 2, we use a response time definition of τ_{95}, which is the time to reach 95% of the total signal level. The larger a sensors τ value, the longer it takes the sensor to respond to a change in ambient conditions. We use regular yo and staircase profiles from VITALS and Trinity Bay missions to do a comparative analysis of the sensor response time against observed temperature gradients (ΔT). The VITALS data are regular glider profiles (yo's). Only a few staircase profiles from VITALS were available and were of low quality and are excluded from this analysis. The Trinity data are mostly regular yo's with nine staircase profiles from 3 days during the deployment (e.g. Figure 3). For both glider tests, we used data for the period after which the sensor had become conditioned to the environment as described earlier.

Figure 4a shows the result of response time fitting against the temperature gradient (ΔT) normalized by the total time of traversing the gradient (dt) and the sensor response (e.g. $\tau_{95,\text{normalized}} = \tau_{95}/\Delta T \times 900$ s). We define ΔT as the total temperature change observed in the interval. We multiply normalized values by 900 s or 15 min to arrive at a set of equally referenced temperature gradient and response time values, all corresponding to the same time interval. We chose this interval based on the response time ($\tau_{95} \approx 15$ min) of the reference sensing system used in the deployments, the Pro CV. We excluded data from time segments shorter than 60 s, longer than 60 min, and $\tau_{95}>900$ s. The VITALS data show increased τ_{95} value scatter for small temperature gradients with no noticeable trend in temperature. The Trinity Bay tests reveal a slight bias in increasing response
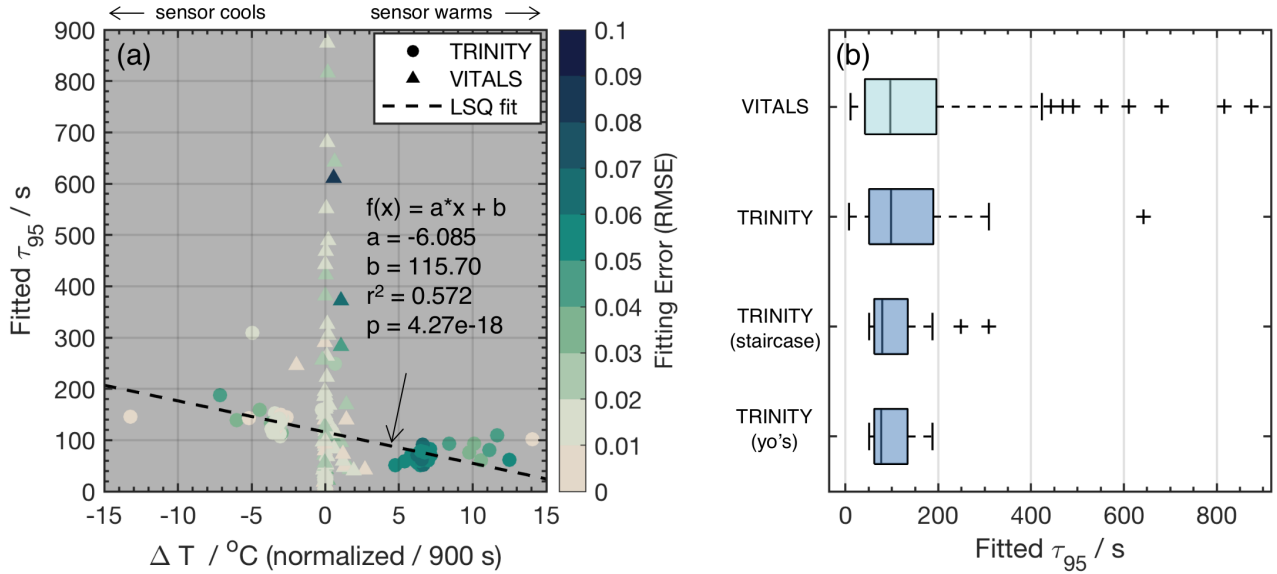
Figure 4. Panel (a) shows the CO_2 optode τ_{95} values vs. temperature gradients ΔT normalized by dt=900 s, color-coded for RMSE of fits to the exponential model $x(t) = (a-b)\exp(-dt/\tau) + b$. Distinct markers are used to differentiate between the VITALS and the Trinity glider data. Dashed line indicated linear least squares (LSQ) fit. Panel (b) shows box plots of the fitted CO_2 optode τ_{95} values from VITALS and Trinity Bay deployments. The Trinity data is divided into staircase profiles and regular yo's.

times with negative temperature gradients. This would indicate the sensor performs better during upcasts than downcasts. We show linear least-squares fits through the Trinity Bay data points, ignoring VITALS data large scatter in the fitting result. Figure 4b summarizes the response time between the deployments. The Trinity data is further divided into the staircase profiles and regular yo's. Contrary to our expectation, the staircase profiles did not noticeably reduce the spread of response times compared to regular yo's. A possible explanation is that the staircase profiles are close to when the sensor was still conditioning, and when the sensor began to show an strange response near the end of the mission. Only one full staircase mission was done in the middle of the deployment (September 10, 2018). A summary of the analysis of the two datasets is given in Table 2.

Based on our analysis, we find a median sensor response time (τ_{95} values) of 79.18 s for the Trinity tests and 96.20 s for the VITALS data, with a mean and standard deviation of 99.24 ± 45.23 s and 169.80 ± 186.55 s respectively. The range of observed response times in Trinity was $50.96 - 309.08$ s. In the VITALS data, the τ_{95} range is much larger ($7.63 - 874.74$). At the same time, ΔT gradients are smaller 0.22 ± 0.0079 ($\bar{x} \pm$ STD) compared to Trinity Bay 2.70 ± 5.62. In the Labrador Sea, stratification is much reduced compared to Trinity Bay, and temperature gradients are typically small $<3\ °C$. One would expect shorter response times for smaller temperature gradients. In Trinity Bay, the sensor encountered water temperatures colder than $0\ °C$. From this analysis alone, it is not clear if there is a permanent effect on the sensor from these cold temperatures. However, Figure 4a does show an increase in response time values when a sensor cools. Not enough data was collected in Trinity Bay to

Table 2. Response time values from glider-based CO_2 Optode tests

Trinity Tests	(units)	(mean)	(median)	(STD)	(min)	(max)
τ_{95}	s	99.24	79.18	45.23	50.96	309.08
ΔT	°C	2.70	6.23	5.62	-13.21	14.06
dt	s	1925.7	1517.0	822.0	314	3226
VITALS						
τ_{95}	s	169.80	96.20	186.55	7.63	874.74
ΔT	°C	0.22	0.0079	0.58	-1.97	2.67
dt	s	944.8	804	490.7	500	3220

see if this temperature gradient bias changes or persists over time. Interestingly the sensor signal (ϕ_{DLR}) range in the VITALS deployment was different than in Trinity Bay, despite the broader temperature range encountered and similar range in pCO_2. It is possible that some bleaching of the foil had occurred from sunlight despite our best efforts to keep the glider surface time to a minimum.

More work will be necessary to develop a proper response time model. We also did not consider applying a boundary layer and fluid flow model for the optode, such as considered by Bittig et al. (2014) for oxygen optodes. Improvements to the sensor response time and more tests are required to evaluate the influence of the flow field on the sensor performance.

3.2 Comparison: Glider and SeaCycler O_2 and CO_2 Observations

A novel aspect of the VITALS deployment was the simultaneous measurement of O_2 and CO_2 from a glider and the SeaCycler profiler, allowing both space and time-varying observations. Given the challenges with validating the glider-based CO_2 optode observations, we used the SeaCycler as an in-situ reference for the glider data. For context, the glider and SeaCycler had about two months of overlapping observations. Figure 5 and Figure 6, show the time series data from SeaCycler and monthly averaged panels from the glider transects. The SeaCycler record is divided into distinct periods coinciding with large changes in at-depth concentration of O_2 and CO_2. The glider measured both the spatial and temporal evolution of the processes captured by SeaCycler. Figure 6, shows monthly averaged panels (approximately 10 glider passes distance-averaged per month) of the glider data. The much lower spatial density of CO_2 glider profiles (at 15-20 km intervals) compared to O_2 (at least 5 km), means that the CO_2 data resolves only spatial features with scales larger than 20 km, compared to a 5 km resolution for O_2. Overall, this region is relatively uniform, with low spatial gradients. Consistent with the SeaCycler observations, we see a flip between concentrations in O_2 and CO_2 between October and November. We also note the different thickness of mixed layer regions across the spatial domain in November.
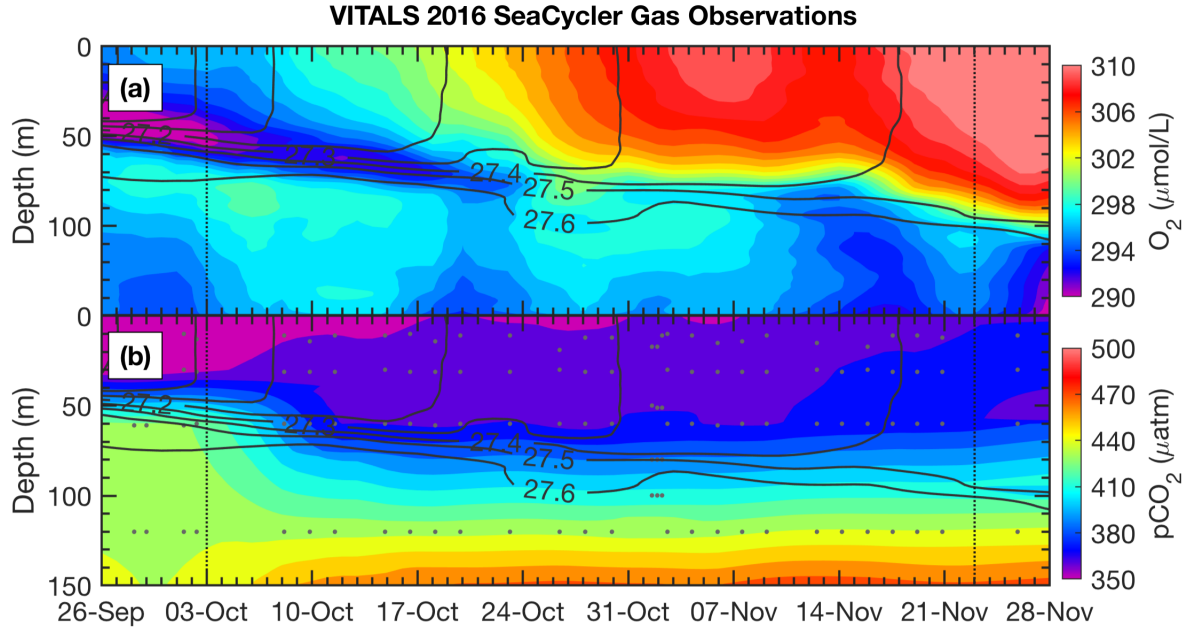
Figure 5. SeaCycler time evolution of (a) O_2 and (b) pCO_2 observations for the joint glider-SeaCycler sampling period with isopycnal anomaly contours overlaid (0.1 $kg \cdot m^{-3}$ spacing). Small grey dots are the depth and time of discrete CO_2 Pro CV measurements by the SeaCycler. Vertical dotted lines indicate the start and end of the joint sampling period.

Table 3. SeaCycler–glider residuals

(parameter)	(mean)	(median)	(STD)	(min)	(max)	(units)
O_2	-0.66	0.64	4.66	-14.30	18.87	μM
pCO_2	17.40	5.92	43.96	-86.45	155.80	μatm
T	0.012	-0.008	0.221	-0.496	0.494	$^\circ C$
S	0.0035	0.0004	0.0320	-0.0719	0.0867	PSU

We intercompare platform observations and compute an in-situ reference point for the glider data from SeaCycler. For the comparison, we only consider data with similar T–S properties using isopycnal matching. We use the glider and SeaCycler data from the joint observing period (3 October to 22 November), binning data across potential density (σ_0) bins of 0.01 kg/m^3 to compute the temperature and salinity residuals from both data sets. If temperature matched to within 0.5°C and salinity to within 0.1 PSU, we allowed these residuals for further comparison of O_2 and pCO_2 between platform observations. The 95% Confidence Interval (CI) is defined as CI= $\bar{x} \pm 1.96$ STD, where $\bar{x}$ is the average of the variable of interest (e.g. pCO_2) and STD is the sample standard deviation. From the matching O_2 and CO_2 data, we plotted the residual cloud across potential density
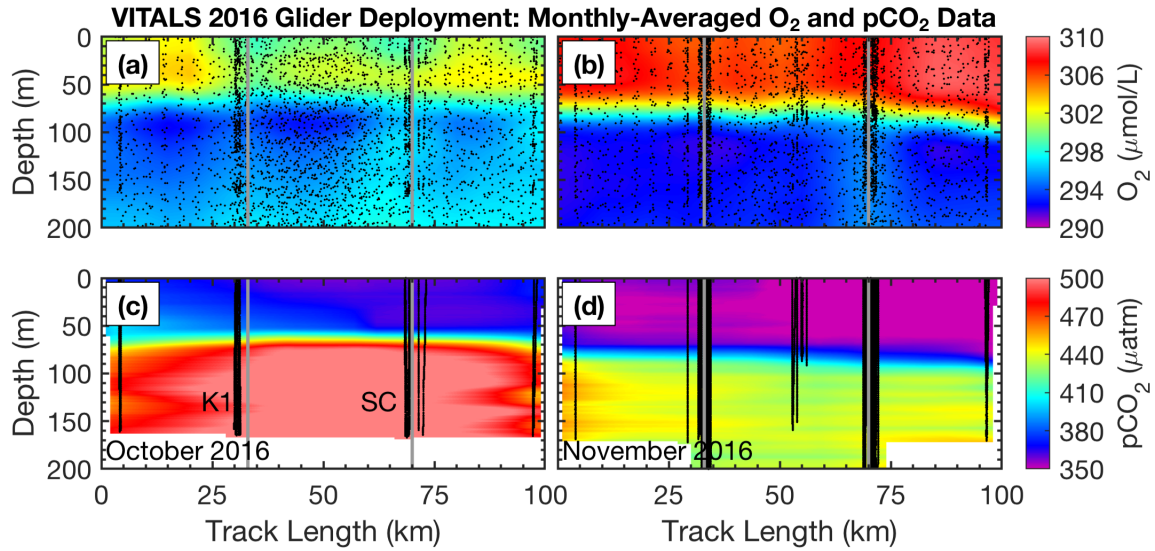
Figure 6. Glider monthly averaged spatial section of (a) O_2 in October and (b) November and for pCO_2 (c) and (d) respectively (along track positions shown in blue inset map in Figure 1). Along-track location of K1 mooring and SeaCycler are indicated with vertical lines as well as individual glider profiles used for plotting. For glider O_2 data only every 25th data point is shown for clarity.

anomaly and found strong duality in residual trends marked by the 27.46 kg/m^3 isopycnal, coinciding with a mixed layer depth (MLD) defined as a change in $\sigma_0 \leq 0.01$ kg/m^3. We used linear, least-squares fits to compute the mean correction of the glider data required to match the SeaCycler (Figure 7), indicating trends above and below the 1027.46 kg/m^3 isopycnal. Significant scatter (± 50 μatm) is observed in CO_2 residuals below the mixed layer. Applying the residual fits from the SeaCycler–glider CO_2 offsets to the glider data as an in-situ reference (Figure 7c), we see reasonable agreement in the mixed layer. Below the mixed layer, the comparison does not fall within the 95% CI limit. However, we see good agreement and relatively little spread (within ± 10 μM) of O_2 data between SeaCycler and glider sensors leading to a good in-situ reference. We observe that the mean (-0.66) and median (-0.64) offsets for O_2 are close compared to the mean (17.40) and median (5.92) offsets for pCO_2. Using the mean and standard deviation of the residuals and the SeaCycler's uncertainty (± 4.17 μM and ± 2 μatm), we estimate the mean offset and uncertainty for glider O_2 and pCO_2 data as -0.66 $\pm$ 6.14 μM and 17.39 $\pm$ 44.01 μatm respectively.

3.3 Glider-Observed Spatial and Temporal Variability

Glider-based observations intrinsically link the spatial and time domain, making it hard to differentiate between these two dimensions. In VITALS, we took the approach of doing repeat glider sections along the same trajectory to capture both the time and spatial evolution of O_2 and CO_2 above and below the mixed layer. A Hovmüller diagram (Figure 8) is useful to look at the propagation of processes across a time and space varying field.
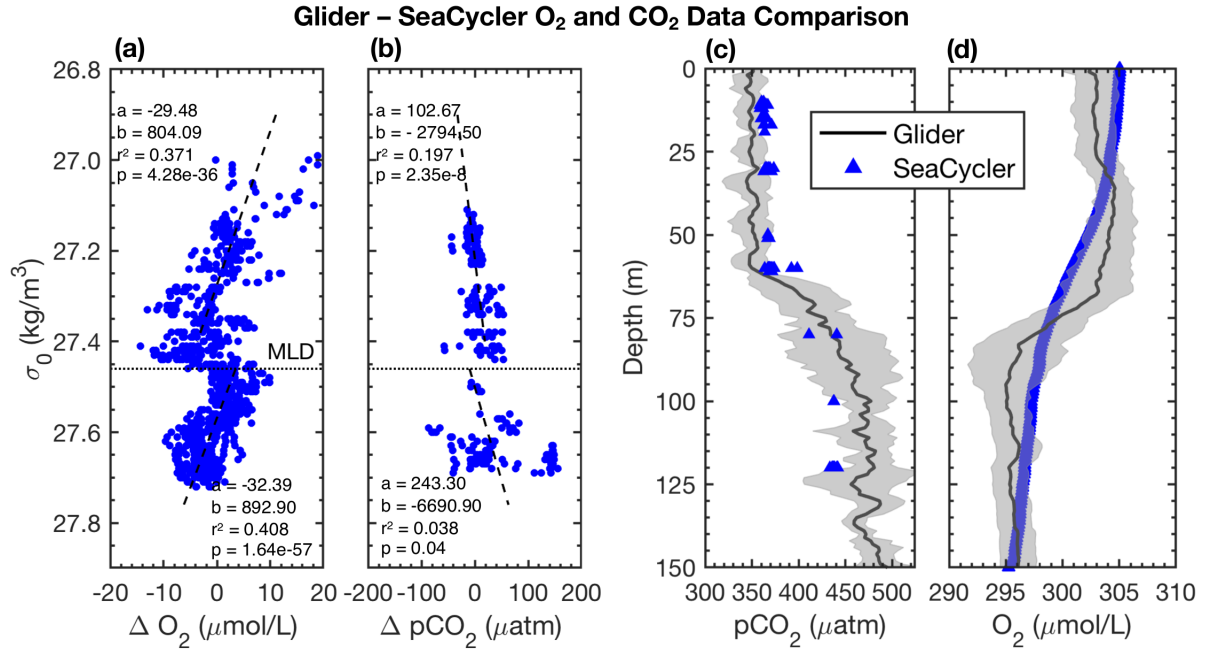
Figure 7. Glider-SeaCycler (a) O_2 and (b) pCO_2 isopycnal-matched residual comparison. Panel (c) and (d) show Glider-SeaCycler corrected depth-averaged pCO_2 and O_2 values with glider 95% CI shown as grey shading for the period from 3 October to 22 November 2016. Blue triangles are mean of SeaCycler measurements for the glider observing period. Dashed horizontal line in panels (a) and (b) is the average density of the mixed layer and dashed lines are linear least-squares fits to the residuals in density space.

305   We are interested in how much variability in O_2 and pCO_2 is captured by the SeaCycler time-series data along the trajectory sampled by the glider, applying the residual fits from Figure 7 to the glider data. Because the in-situ comparison between the glider and SeaCycler CO_2 data was better at the surface, we only consider data within the mixed-layer (0 – 20 m). We compute surface O_2 and pCO_2 anomalies with respect to the SeaCycler by subtracting corresponding SeaCycler surface, daily averaged data from the glider record. We use the objective interpolation technique described earlier, interpolating the data using an

310 exponential weighting function to fill in gaps along a 50 day (3 October – 22 November) and 100 km grid. We could have used linear interpolation for the glider oxygen data but decided to keep mapping methods consistent between O_2 and pCO_2 data. A drawback of this technique is that it can show artificial variability in the resultant interpolated surface. We applied a low pass filter removing signals shorter than 3-days (time of glider transect) and 4-km (average distance between dives). We used larger scales of 40 km for the glider pCO_2 data. Dots indicate the location of data samples.

315   Figure 8 shows the spatial and temporal anomalies of the glider data referenced to the SeaCycler data. We note that the scales of the anomalies are within the estimated uncertainty of the glider data. We see that only a few spatial features are visible in O_2 data, and the overall spatial structure is not as pronounced as the time variability. Towards the beginning of the record, there is a distinctly more oxygenated zone between K1 mooring and SeaCycler. This could mean that perhaps the low oxygen levels
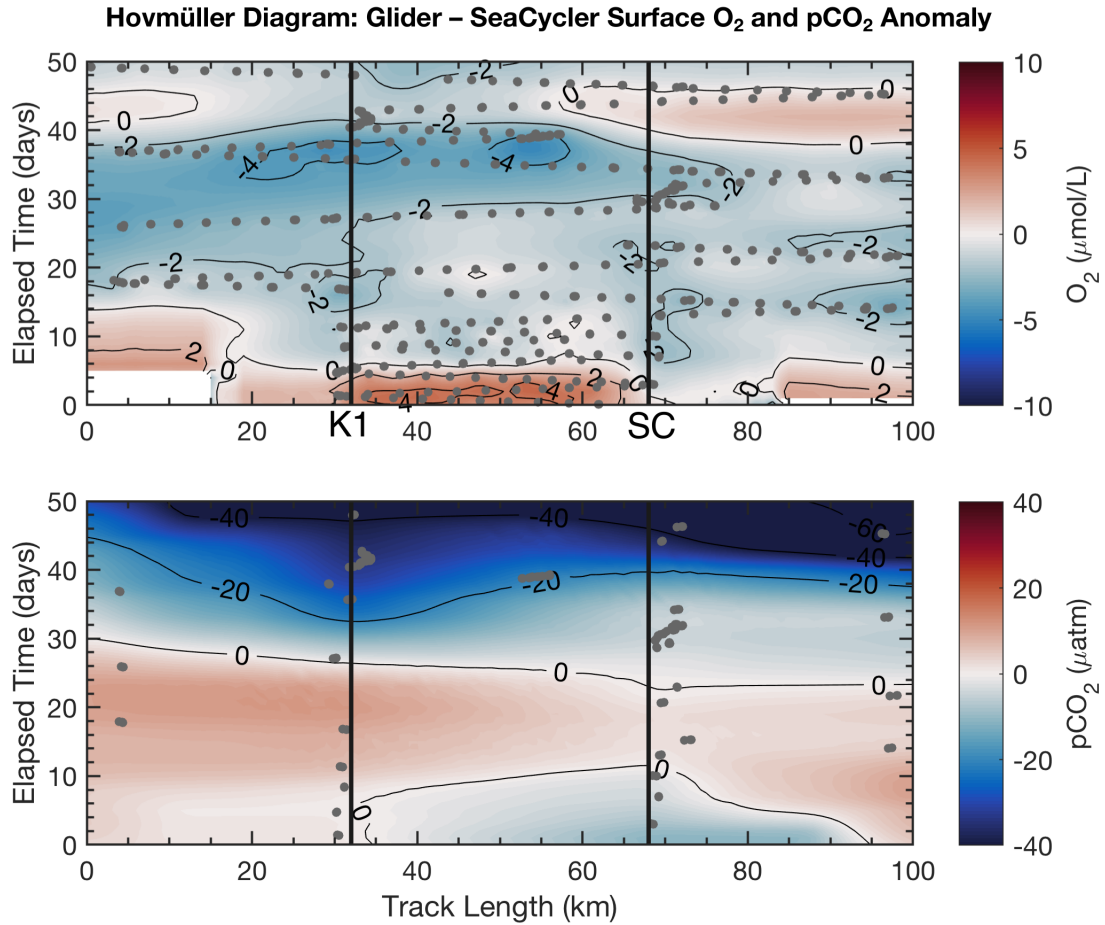
Figure 8. Glider Hovmüller diagram, for O_2 (top panel) and pCO_2 (bottom panel) surface averaged data (0–20 m) with SeaCycler data removed for period 3 October – 22 November, 2016. Dots indicate the location of data samples. Location of K1 and SeaCycler (SC) moorings shown in black.

measured by SeaCycler from August to October had more considerable spatial variability. There are different patterns between
320   moorings. Near SeaCycler, the O_2 levels are elevated by 2 μM compared to the K1 mooring, while data near the K1 mooring show lower oxygen levels over time. Towards the second half of the glider record, as storm activity increases in November, the spatial domain becomes smoother with spatial variability reduced to $\pm 1 \mu$M. The glider sampled O_2 daily and along the entire track length, while the CO_2 optode was only sampled at select locations and on average every 2–3 days. The CO_2 glider data sampling was too sparse and required too much smoothing to resolve signals smaller than the seasonal cycle. Therefore,
325   the data appears very uniform along the track length. However, this type of direct comparison between platforms will become increasingly important, especially as sensor improvements improve data accuracy. For future glider deployments, this approach

may also help to achieve long term monitoring capability, re-calibrating sensors that suffer from drift and help with quality control of mobile platform data.

To separate temporal and spatial variability from each other, we can treat each dimension independently, comparing their autocorrelation scales against each other to measure the variability observed. For this analysis, we did not include the glider observations of CO_2 due to the sparse sampling across space and time. However, the scales that drive variability in T, S and O_2 data also affect the dynamics of CO_2 solubility and the extent and strength of carbon sinks (Li et al., 2019; Atamanchuk et al., 2020). We use the definition from Chatfield (1998) of the correlogram or autocorrelation $r(k)$ as a function of lag k.

$$r(k) = \frac{\sum_{t=1}^{N-k}(x_t - \bar{x})(x_{t+k} - \bar{x})}{\sum_{t=1}^{N}(x_t - \bar{x})^2} \tag{3}$$

Here, x_t denotes any quantity of interest (e.g. T, S or O_2) and $\bar{x}$ is the average of x_t along dimension t, k can denote either spatial or temporal lags and N is the total number of samples along each dimension. We detrended the gridded space-time glider data to remove non-stationary time, and spatial trends following Chatfield (1998) and compute the autocorrelation in space and time lags (km and days) for S, T and O_2. We repeat this analysis across the potential density anomaly contours of 27.3, 27.7 and 27.75 kg/m^3, corresponding closely to surface, intermediate and deepest water regions surveyed by the glider. We include this analysis to the 95% CI bounds defined previously as CI$= \bar{x} \pm 1.96$ STD, where STD is computed from the range of correlation functions calculated for the whole isopycnal glider space-time data-set.

The autocorrelation function for T, S and O_2 (Figure 9) show different spatial and time scales across all properties between surface and deeper water layers. T, S and O_2 have similar spatial first zero-crossings of approximately 7–10 km for intermediate and deep waters (27.7–27.75 kg/m^3). O_2 and T also have similar scales (6–7 km) for surface mixed layer waters (27.3 kg/m^3). S has the first zero crossings at scales around 10 km at the surface mixed layer. CI limits on T and O_2 are more similar in intermediate–depth waters and differ at the surface, where T and S seem to be more tightly related than oxygen. Across T, S and O_2, the CI limit is constrained by 23 km on the upper end and 3 km on the lower end.

Time scales vary more between properties than do spatial scales. T, O_2 and S have similar temporal correlation at the surface (11–13 days). On the other hand, O_2 has very different intermediate-depth scales (16 days) compared to T and S (7–11 days). These results suggest that there are different underlying dynamics between the surface and intermediate–deep water layers that drive T, S and O_2 time scales as observed in the temporal SeaCycler record (Figure 5. The CI time–scale limits for O_2 are also different compared to T and S in intermediate layers. The temporal scales for O_2 in the intermediate depth layer fall within the mean of the CI interval (6–29 days), suggesting that the distribution of correlation values centred around this range of scales. On the other hand, T, S scales are closer to the lower limit of the 95% CI bounds (4–24 days).

Overall, spatial scales vary less dramatically between density layers than temporal scales. The presence of energetic shifting of density layers (every 3 to 5 hours) in the intermediate depth waters would force spatial scales to be small. The glider takes about 3 hours to complete a full dive-climb cycle over a distance of 3–4 km. As the glider begins the next dive-climb cycle, the glider will likely see a shift in the depth of intermediate-depth density layers as it will be between 3 to 5 hours since it first measured the same density layer. A study by Sathiyamoorthy and Moore (2002) found similar time scales of T and S of around two weeks at the surface, explaining the observed time scales from buoyancy fluxes observed at OWS Bravo data. They link
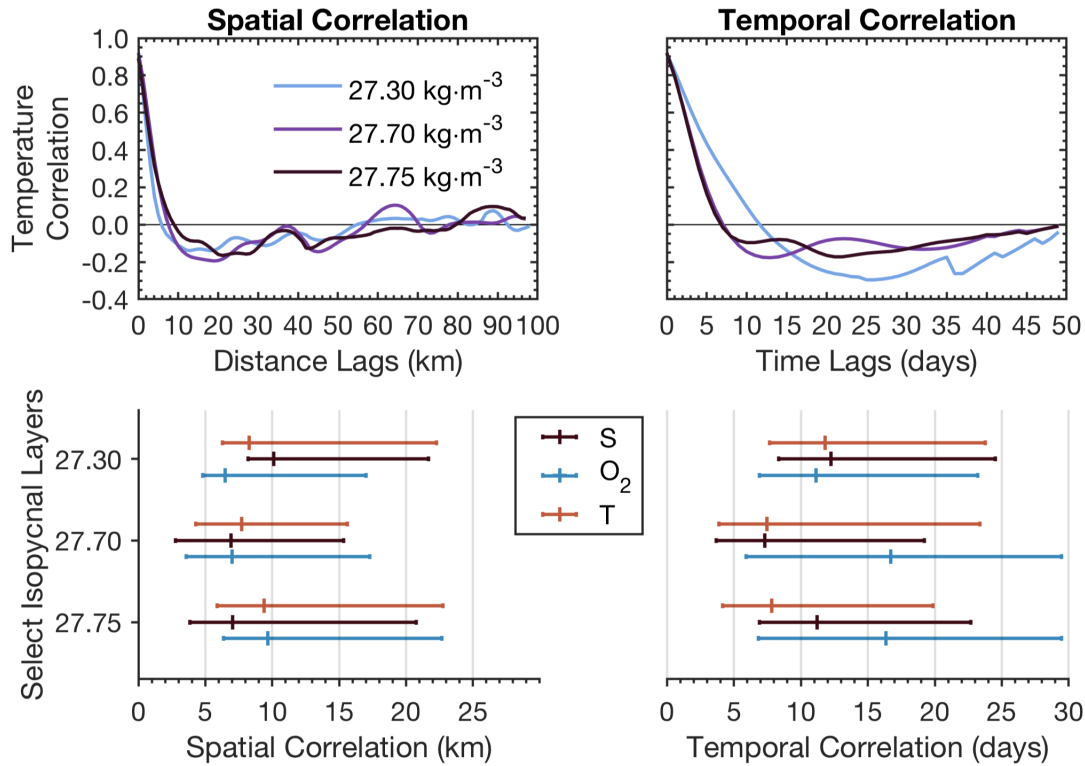
Figure 9. Upper panels show example autocorrelation functions for T as a function of distance and time lags. Lower panels summarize zero–crossings for T, S and O$_2$ in space and time lags for shown isopycnals together with 95% CI bounds.

correlation scales in T and S to cyclonic airflow regime changes in the North Atlantic, suggesting storm activity at roughly two weeks in the Labrador Sea in the fall. Their result indicates that storms occurring every few weeks are primarily responsible for changes in T, S and O$_2$ in the surface layer.

The significant difference in time scales between T–S (7–11 days) and O$_2$ (16 days) across intermediate-deep layers, however, is not intuitive. Changes in O$_2$ may be related to biogenic activity with a 2–week period. However, this would not explain changes in T and S. We cannot be sure without further insights from direct observations into the fall and early winter in the Labrador Sea. The small spatial scales of around 10 km, does suggest highly variable changes. Due to temperature dependence, this should also result in localized changes in CO$_2$ cycling. We still do not know exactly how much carbon is taken up in the Labrador Sea, and understanding the impact of localized changes to solubility pumps is an important step. Small-scale spatial variability of pCO$_2$ for CO$_2$ uptake is important. To distinguish the changes in the strength of CO$_2$ uptake, we need to continue to improve spatial observations of CO$_2$ concentrations in these regions.

We are aware that neither time nor spatial scale results can be interpreted without being mindful of the glider platform's limitations due to aliasing (Rudnick, 2016) and the uncertainty of the collected data itself. However, compared to contemporary

studies in other water regions, our scale results point to much higher variability across all properties, including CO_2 along time-space dimensions in the Labrador Sea. For reference, traditional annual ship sampling programs in the Labrador Sea, such as the AR7W section, cover the track of the whole glider mission in a fraction of time but have spatial gaps on the order of 10s of nautical miles between stations – well above the average spatial correlation length scales observed by our glider mission. Other platforms such as ARGO floats cover larger areas but lack the glider platforms' targeted sampling capability. Therefore gliders play an important role in constructing an effective observing strategy to resolve the fine-scale processes missed by other platforms.

4   Conclusions

In this study, we show data and results of testing a pCO_2 optode sensor (Aanderaa model 4979) on a glider. However, improving glider-based CO_2 observations is essential to capture the evolving space-time dynamics of carbon sinks in the ocean. We addressed three questions in this paper: (1) How suitable is the novel CO_2 optode for glider-based applications? (2) How can multiple autonomous platforms be used to help improve sensor data? (3) How combined moored and mobile platforms can resolve scales of temporal and spatial variability? We view answering these questions as essential to advance current sensor technology and glider-based CO_2 observing capabilities.

Our deployments were the first glider-based tests of the novel pCO_2 optode. We deployed the glider in an initial test as part of a mission to collect data between two moorings in the central Labrador Sea. From initial evaluations of this mission and questions about the sensor performance in small temperature gradients (<3 °C) characteristic for the Labrador Sea, we re-deployed the glider in Trinity Bay, Newfoundland, where temperature gradients are large (>10 °C). For the second test, we focused on extensive initial tank comparisons between the CO_2 optode and reference sensors using a large saltwater tank that allowed us to submerge all systems at once. We also attempted various glider missions such as the staircase mission vs. regular glider profiles to differentiate between the sensor performance. Several difficulties in using the sensor on a glider were observed, such as drift and long response times. In both missions, the sensor foil conditioning effect is initially observed by a steep exponential curve, flattening after some time. In the VITALS mission, the sensor showed strong conditioning effects in the first cycle of the deployment and stabilized after about a month into the deployment. We calculated an initial conditioning offset of 1275 μatm by comparing the sensor data with atmospheric measurements and SeaCycler. For the Trinity tests, the sensor stabilized after about 4 days (offset of 994 μatm), but the sensor showed a non-linear depth-dependent response towards the end of the mission, and almost two days of data had to be excluded.

From the VITALS Labrador Sea deployment, we calculated average response times of the sensor (τ_{95}) 169.80 $\pm$ 186.55 s for temperature gradients of 0.22 $\pm$ 0.58 °C. In Trinity Bay, with larger temperature gradients of 2.70 $\pm$ 5.62 °C, we find response times are 99.24 $\pm$ 45.23 s. We were able to correct the sensor's response time, applying methods similar to those in Fiedler et al. (2013). However, more tests are required to validate our results and characterize the influence of other factors, such as the boundary layer in the sensor's flow field. We identified a large scatter in sensor response times for small temperature gradients in the Labrador Sea data. We also detected a small bias in performance towards positive temperature gradients, suggesting the

sensor performs better in upcasts than in downcasts. Presently the sensor does not yet have the reliability to measure pCO_2 from a glider. The sensor's drift and conditioning are not well understood, and not much prior published test results are available for comparison. The sensing foil likely needs more work to improve stability. The optode has some key strengths, such as its small size, easy integration and low power consumption. If the foil stability and sensitivity could be improved, the sensor could become a desirable candidate for ocean gas measurements similar to the commonly used O_2 optode.

In the Labrador Sea mission, we demonstrated how to use the SeaCycler CO_2 PRO-CV instrument as an in-situ mid-deployment reference point to validate the glider CO_2 data. Our corrections for the experimental glider CO_2 optode, using SeaCycler data, yielded a robust surface mixed layer correction of the glider data, but the subsurface data remained noisy. For the more reliable O_2 optode, this method worked well, and agreement in data to within $\pm$ 10 μM was achieved. Using the residuals from the glider–SeaCycler comparison, we estimate the mean offset and uncertainty for glider O_2 and pCO_2 data as -0.66 $\pm$ 6.14 μM and 17.39 $\pm$ 44.01 μatm respectively.

The unique capability to synchronize and synthesize data from different sensor systems allowed us to investigate the high-resolution glider observations' spatial and temporal character. The repeat sections of the glider yielded a dynamic picture across all measured properties (T, S, O_2, CO_2) in both time and space. On average, we observed spatial scales across measured properties of less than 10 km and temporal scales of 15 days or less. Our results agreed with previous studies pointing to increased storminess in the fall to explain the roughly 2-week period in time scales. We lacked enough data also to quantify time and spatial scales of pCO_2. However, given the strong dependence between T and CO_2, our results point to the importance of having targeted winter-time glider observations to observe small-scale spatial variability of CO_2 cycling. Overall, our analysis points to much finer scale and localized processes than commonly described in the literature or captured by other observing systems, underlining the importance of repeat glider observations in this region.

These results clearly show that there remain challenges to achieve reliable glider-based CO_2 observations. The CO_2 optode sensor does not yet meet the targets for ocean acidification observations, as discussed by Newton et al. (2015). In the meantime, one option is to measure pH rather than CO_2. The work by Saba et al. (2018), testing an ISFET pH sensor on a Slocum glider, found accuracy to be better than 0.011 pH units and is indeed very promising. These sensors are already in regular use on BGC Argo floats. Calculation of pCO_2 from pH requires knowledge of at least one other carbonate parameter. On the other hand, pH vs pCO_2 relationships measured at fixed platforms like SeaCycler could support this calculation. One limitation of the pH sensor is that one could not use the data to measure air-sea gas exchange because it is not a direct measurement of pCO_2. No matter which sensor one chooses, we believe that in-situ referencing between platforms can add value to existing and future sensors deployments on autonomous platforms such as floats, gliders and moorings.

Data availability. VITALS 2016 glider deployment data is available at https://doi.org/10.17882/62358. Processed CO_2 optode data from both deployments is available from the authors upon request.

Appendix A: DFO Sample Analysis

Niskin bottle samples were collected in the lab in 500 mL BOD bottles. They were poisoned 100 μL of saturated Mercuric-Chloride ($HgCL_2$) and allowed to warm in a temperature-controlled bath (25°C $\pm$ 0.1 °C) before analysis. Winkler titrations were performed on water samples to calculate oxygen concentrations. Uncertainty of the Winkler titrations were $\pm$0.01 ml/L or $\pm$0.44 μM ($\pm$ 1 STD). TA and DIC were estimated from coulometry (Johnson et al., 1993) and potentiometric titration (Mintrop et al., 2000). Equipment used to estimate TA and DIC was as follows: VINDTA 3D TA–DIC analyzer connected to a coulometer (UIC, USA, model 5015O), VINDTA 3S (TA) analyzer using open cell differential potentiometry equipped with a reference (Metrohm, Canada, model 6.0729.100) and pH glass (Thermo-Orion, Canada, model 8101BNWP Ross half-cell) electrode, which were both referenced against a grounded platinum electrode. Based on TA and DIC, pCO$_2$ was calculated using CO2calc (Robbins et al., 2010), with CO$_2$ equilibrium constants from (Mehrbach et al., 1973; Dickson and Millero, 1987), total boron constant (Lee et al., 2010), and KHSO4 constants (Dickson, 1990). Analytical instrumentation at DFO undergoes a daily operational evaluation of accuracy using CRM's, from which estimated uncertainty for DIC and TA measurements are 3 and 4 μmol/kg, respectively (Gary Maillet,gary.maillet@dfo-mpo.gc.ca, *personal communications*). Including the TA-DIC inputs' uncertainty into CO2calc, we estimate pCO$_2$ uncertainty as $\pm$4.48 μatm.

Author contributions. NVOB carried out research and initiated the paper, BDY and DA contributed research ideas. All authors contributed to revisions and comments of the paper.

Competing interests. None declared.

Acknowledgements. We thank Mingxi Zhou, Mark Downey, for fieldwork support, Chris L'Esperance, with sensor calibrations, Fisheries and Oceans Canada for access to their saltwater-tank facility and Gary Maillet for help with water sample analysis. We acknowledge funding from the National Science and Engineering Research Council (NSERC), Climate Change and Atmospheric Research (CCAR) network.

References

Atamanchuk, D., Tengberg, A., Thomas, P. J., Hovdenes, J., Apostolidis, A., Huber, C., and Hall, P. O.: Performance of a lifetime-based
optode for measuring partial pressure of carbon dioxide in natural waters, Limnology and Oceanography: Methods, 12, 63–73, 2014.

Atamanchuk, D., Kononets, M., Thomas, P. J., Hovdenes, J., Tengberg, A., and Hall, P. O.: Continuous long-term observations of the
carbonate system dynamics in the water column of a temperate fjord, Journal of Marine Systems, 148, 272–284, 2015.

Atamanchuk, D., Koelling, J., Send, U., and Wallace, D. W. R.: Rapid transfer of oxygen to the deep ocean mediated by bubbles, Nature
Geoscience, pp. 1752–0908, 2020.

Avsic, T., Karstensen, J., Send, U., and Fischer, J.: Interannual variability of newly formed Labrador Sea Water from 1994 to 2005, Geophys-
ical Research Letters, 33, 2006.

Bakker, D. C. E., Pfeil, B., Landa, C. S., Metzl, N., O'Brien, K. M., Olsen, A., Smith, K., et al.: A multi-decade record of high-quality fCO$_2$
data in version 3 of the Surface Ocean CO$_2$ Atlas (SOCAT), Earth System Science Data, 8, 383–413, https://www.earth-syst-sci-data.net/
8/383/2016/, 2016.

Bittig, H. C., Fiedler, B., Scholz, R., Krahmann, G., and Körtzinger, A.: Time response of oxygen optodes on profiling platforms and its
dependence on flow speed and temperature, Limnology and Oceanography: Methods, 12, 617–636, 2014.

Borges, A., Alin, S., Chavez, F., Vlahos, P., Johnson, K., Holt, J., Balch, W., Bates, N., Brainard, R., Cai, W., et al.: A global sea surface carbon
observing system: Inorganic and organic carbon dynamics in coastal oceans, Proceedings of OceanObs'09: Sustained Ocean Observations
and Information for Society, 2, 2010.

Broecker, W. S.: The Great Ocean Conveyor, Oceanography, 4, 79–89, 1991.

Chatfield, C.: The Analysis of Time Series: An Introduction, Chapman and Hall/CRC, 5 edn., 1998.

Clarke, J. S., Achterberg, E. P., Connelly, D. P., Schuster, U., and Mowlem, M.: Developments in marine pCO$_2$ measurement technology;
towards sustained in situ observations, TrAC Trends in Analytical Chemistry, 88, 53–61, 2017a.

Clarke, J. S., Humphreys, M. P., Tynan, E., Kitidis, V., Brown, I., Mowlem, M., and Achterberg, E. P.: Characterization of a time-domain dual
lifetime referencing pCO$_2$ optode and deployment as a high-resolution underway sensor across the high latitude North Atlantic Ocean,
Frontiers in Marine Science, 4, 396, 2017b.

Cohen, A. L. and Holcomb, M.: Why corals care about ocean acidification: uncovering the mechanism, Oceanography, 22, 118–127, 2009.

DeGrandpre, M., Körtzinger, A., Send, U., Wallace, D. W., and Bellerby, R.: Uptake and sequestration of atmospheric CO$_2$ in the Labrador
Sea deep convection region, Geophysical Research Letters, 33, 2006.

Dickson, A. G.: Standard potential of the reaction: AgCl(s) + 12H2(g) = Ag(s) + HCl(aq), and and the standard acidity constant
of the ion HSO4- in synthetic sea water from 273.15 to 318.15 K, The Journal of Chemical Thermodynamics, 22, 113–127,
https://doi.org/https://doi.org/10.1016/0021-9614(90)90074-Z, 1990.

Dickson, A. G. and Millero, F. J.: A comparison of the equilibrium constants for the dissociation of carbonic acid in seawater media, Deep-Sea
Research, Part A: Oceanographic Research Papers, 34, 1733–1743, https://doi.org/10.1016/0198-0149(87)90021-5, 1987.

Doney, S. C., Lima, I., Feely, R. A., Glover, D. M., Lindsay, K., Mahowald, N., Moore, J. K., and Wanninkhof, R.: Mechanisms governing
interannual variability in upper-ocean inorganic carbon system and air–sea CO$_2$ fluxes: Physical climate and atmospheric dust, Deep Sea
Research Part II: Topical Studies in Oceanography, 56, 640–655, 2009.

Fiedler, B., Fietzek, P., Vieira, N., Silva, P., Bittig, H. C., and Körtzinger, A.: In situ CO$_2$ and O$_2$ measurements on a profiling float, Journal
of Atmospheric and Oceanic Technology, 30, 112–126, 2013.

495   Fontela, M., García-Ibáñez, M. I., Hansell, D. A., Mercier, H., and Pérez, F. F.: Dissolved organic carbon in the North Atlantic Meridional Overturning Circulation, Scientific reports, 6, 26 931, 2016.

Friedlingstein, P., Jones, M. W., O'Sullivan, M., Andrew, R. M., Hauck, J., Peters, G. P., Peters, W., Pongratz, J., Sitch, S., Le Quéré, C., et al.: Global Carbon Budget 2019, Earth System Science Data, 11, 1783–1838, https://doi.org/10.5194/essd-11-1783-2019, 2019.

Fritzsche, E., Staudinger, C., Fischer, J. P., Thar, R., Jannasch, H. W., Plant, J. N., Blum, M., Massion, G., Thomas, H., Hoech, J., et al.: A
500   validation and comparison study of new, compact, versatile optodes for oxygen, pH and carbon dioxide in marine environments, Marine Chemistry, 207, 63–76, 2018.

Garau, B., Ruiz, S., Zhang, W. G., Pascual, A., Heslop, E., Kerfoot, J., and Tintoré, J.: Thermal lag correction on Slocum CTD glider data, Journal of Atmospheric and Oceanic Technology, 28, 1065–1071, 2011.

Goodin, W. R., McRae, G. J., and Seinfeld, J. H.: A Comparison of Interpolation Methods for Sparse Data: Application to Wind and
505   Concentration Fields, Journal of Applied Meteorology (1962-1982), 18, 761–771, http://www.jstor.org/stable/26179119, 1979.

Gourcuff, C.: ANFOG Slocum Oxygen data: new computation, 2014.

Guinotte, J. and Fabry, V. J.: The threat of acidification to ocean ecosystems, Ocean acidification—from ecological impacts to policy Opportunities, 25, 2, 2009.

Jiang, Z.-P., Hydes, D. J., Hartman, S. E., Hartman, M. C., Campbell, J. M., Johnson, B. D., Schofield, B., Turk, D., Wallace, D., Burt, W. J.,
510   et al.: Application and assessment of a membrane-based pCO_2 sensor under field and laboratory conditions, Limnology and Oceanography: Methods, 12, 264–280, 2014.

Johnson, K., Wills, K., Butler, D., Johnson, W., and Wong, C.: Coulometric total carbon dioxide analysis for marine studies: maximizing the performance of an automated gas extraction system and coulometric detector, Marine Chemistry, 44, 167–187, https://doi.org/https://doi.org/10.1016/0304-4203(93)90201-X, marine Physical Chemistry - in memory of the contributions made to the
515   field by Dr. Ricardo Pytkowicz, 1993.

Johnson, K. S., Berelson, W. M., Boss, E. S., Chase, Z., Claustre, H., Emerson, S. R., Gruber, N., Körtzinger, A., Perry, M. J., and Riser, S. C.: Observing biogeochemical cycles at global scales with profiling floats and gliders: prospects for a global array, Oceanography, 22, 216–225, 2009.

Johnson, K. S., Jannasch, H. W., Coletti, L. J., Elrod, V. A., Martz, T. R., Takeshita, Y., Carlson, R. J., and Connery, J. G.: Deep-Sea DuraFET:
520   A pressure tolerant pH sensor designed for global sensor networks, Analytical chemistry, 88, 3249–3256, 2016.

Johnson, K. S., Plant, J. N., Coletti, L. J., Jannasch, H. W., Sakamoto, C. M., Riser, S. C., Swift, D. D., Williams, N. L., Boss, E., Haëntjens, N., et al.: Biogeochemical sensor performance in the SOCCOM profiling float array, Journal of Geophysical Research: Oceans, 122, 6416–6436, 2017.

Khatiwala, S., Tanhua, T., Mikaloff Fletcher, S., Gerber, M., Doney, S., Graven, H., Gruber, N., McKinley, G., Murata, A., Ríos, A., et al.:
525   Global ocean storage of anthropogenic carbon, Biogeosciences, 10, 2169–2191, 2013.

Koelling, J., Wallace, D. W., Send, U., and Karstensen, J.: Intense oceanic uptake of oxygen during 2014–2015 winter convection in the Labrador Sea, Geophysical Research Letters, 44, 7855–7864, 2017.

Lavender, K. L., Davis, R. E., and Owens, W. B.: Observations of open-ocean deep convection in the Labrador Sea from subsurface floats, Journal of Physical Oceanography, 32, 511–526, 2002.

530   Lee, K., Kim, T., Byrne, R. H., Millero, F. J., Feely, R. A., and Liu, Y.: The universal ratio of boron to chlorinity for the North Pacific and North Atlantic oceans, Geochimica et Cosmochimica Acta, 74, 1801–1811, 2010.

Li, B., Watanabe, Y., Hosoda, S., Sato, K., and Nakano, Y.: Quasi-Real-Time and High-Resolution Spatiotemporal Distribution of Ocean Anthropogenic CO_2, Geophysical research letters, 46, 4836–4843, 2019.

Mehrbach, C., Culberson, C. H., Hawley, J. E., and Pytkowicx, R. M.: Measurement of the apparent dissociation constants of carbonic acid in seawater at atmospheric pressure, Limnology and Oceanography, 18, 897–907, https://doi.org/10.4319/lo.1973.18.6.0897, 1973.

Miloshevich, L. M., Paukkunen, A., Vömel, H., and Oltmans, S. J.: Development and validation of a time-lag correction for Vaisala radiosonde humidity measurements, Journal of Atmospheric and Oceanic Technology, 21, 1305–1327, 2004.

Mintrop, L., Pérez, F., González-Dávila, M., Santana-Casiano, M., and Körtzinger, A.: Alkalinity determination by potentiometry: Intercalibration using three different methods, Ciencias Marinas, 2000.

Newton, J., Feely, R., Jewett, E., Williamson, P., and Mathis, J.: Global ocean acidification observing network: requirements and governance plan, Tech. rep., GOA-ON, http://www.goa-on.org/docs/GOA-ON_plan_print.pdf, 2015.

Okazaki, R. R., Sutton, A. J., Feely, R. A., Dickson, A. G., Alin, S. R., Sabine, C. L., Bunje, P. M., and Virmani, J. I.: Evaluation of marine pH sensors under controlled and natural conditions for the Wendy Schmidt Ocean Health X-PRIZE, Limnology and Oceanography: Methods, 15, 586–600, 2017.

Peeters, F., Atamanchuk, D., Tengberg, A., Encinas-Fernández, J., and Hofmann, H.: Lake metabolism: Comparison of lake metabolic rates estimated from a diel CO_2 and the common diel O_2 technique, PloS one, 11, e0168 393, 2016.

Robbins, L. L., Hansen, M. E., Kleypas, J. A., and Meylan, S. C.: CO2calc – a user-friendly seawater carbon calculator for Windows, Max OS X, and iOS (iPhone), US Geological Survey open-file report, 1280, 2010, 2010.

Rudnick, D. L.: Ocean research enabled by underwater gliders, Annual Review of Marine Science, 8, 519–541, 2016.

Saba, G. K., Wright-Fairbanks, E., Miles, T. N., Chen, B., Cai, W.-J., Wang, K., Barnard, A. H., Branham, C. W., and Jones, C. P.: Developing a profiling glider pH sensor for high resolution coastal ocean acidification monitoring, in: OCEANS 2018 MTS/IEEE Charleston, pp. 1–8, IEEE, 2018.

Sabine, C. L., Feely, R. A., Gruber, N., Key, R. M., Lee, K., Bullister, J. L., Wanninkhof, R., Wong, C., Wallace, D. W., Tilbrook, B., et al.: The oceanic sink for anthropogenic CO_2, science, 305, 367–371, 2004.

Sathiyamoorthy, S. and Moore, G.: Buoyancy flux at ocean weather station Bravo, Journal of Physical Oceanography, 32, 458–474, 2002.

Schillinger, D. J., deYoung, B., and Foley, J. S.: Physical and Biological Tow-Yo Data from Trinity Bay, July 2000, Tech. rep., Memorial University, 2000.

Send, U., Fowler, G., Siddall, G., Beanlands, B., Pittman, M., Waldmann, C., Karstensen, J., and Lampitt, R.: SeaCycler: A moored open-ocean profiling system for the upper ocean in extended self-contained deployments, Journal of Atmospheric and Oceanic Technology, 30, 1555–1565, 2013.

Takeshita, Y., Martz, T. R., Johnson, K. S., and Dickson, A. G.: Characterization of an ion sensitive field effect transistor and chloride ion selective electrodes for pH measurements in seawater, Analytical chemistry, 86, 11 189–11 195, 2014.

Tengberg, A., Hovdenes, J., Andersson, H. J., Brocandel, O., Diaz, R., Hebert, D., Arnerich, T., Huber, C., Körtzinger, A., Khripounoff, A., et al.: Evaluation of a lifetime-based optode to measure oxygen in aquatic systems, Limnology and Oceanography: Methods, 4, 7–17, 2006.

Testor, P., deYoung, B., Rudnick, D., Glenn, S., Hayes, D., Lee, C. M., Pattiaratchi, C., Hill, K., Heslop, E., Turpin, V., et al.: Ocean Gliders: a component of the integrated GOOS, in review, 2019.

Tittensor, D. P., deYoung, B., and Foley, J. S.: Analysis of Physical Oceanographic Data from Trinity Bay, May-August 2002, Tech. rep., Memorial University, 2002.

570   Uchida, H., Kawano, T., Kaneko, I., and Fukasawa, M.: In situ calibration of optode-based oxygen sensors, Journal of Atmospheric and Oceanic Technology, 25, 2271–2281, 2008.

van Heuven, S. M., Hoppema, M., Jones, E. M., and de Baar, H. J.: Rapid invasion of anthropogenic CO_2 into the deep circulation of the Weddell Gyre, Philosophical Transactions of the Royal Society A: Mathematical, Physical and Engineering Sciences, 372, 20130 056, 2014.

575   Volk, T. and Hoffert, M. I.: Ocean carbon pumps: Analysis of relative strengths and efficiencies in ocean-driven atmospheric CO_2 changes, The carbon cycle and atmospheric CO_2: natural variations Archean to present, pp. 99–110, 1985.

von Oppeln-Bronikowski, N.: Glider data from VITALS 2016 deployment, https://doi.org/https://doi.org/10.17882/62358, https://www.seanoe.org/data/00512/62358/, 2019.

Zeebe, R. E., Ridgwell, A., and Zachos, J. C.: Anthropogenic carbon release rate unprecedented during the past 66 million years, Nature
580   Geoscience, 9, 325, 2016.